First Demonstration of 28 GHz and 39 GHz Transmission Lines and Antennas on Glass Substrates for 5G Modules

Atom O. Watanabe, Muhammad Ali, Bijan Tehrani, Jimmy Hester,
P. Markondeya Raj, Venky Sundaram, Manos M. Tentzeris, and Rao R. Tummala
3D System Packaging Research Center
Georgia Institute of Technology
Atlanta, GA, USA
email: atom@gatech.edu

Hiroyuki Matsuura
NGK Spark Plug Co., Ltd.
Aichi, Japan
email: hiro-matsuura@mg.ngkntk.co.jp

Tomonori Ogawa
Asahi Glass Company
Tokyo, Japan
email: togawa@agcem.com

***Abstract*— High-performance and ultra-miniaturized mm-wave building block structures were demonstrated on panel-scale processed 3D glass packages for high-speed 5G communication standards at 28 and 39 GHz bands. To demonstrate the benefits of glass for 5G communications, various topologies of microstrip-fed patch antennas for different resonant frequencies and compact conductor-backed co-planar waveguides were modeled and designed for high bandwidth and efficiency in the mm-wave bands. The simulation results for insertion loss, antenna gain, and bandwidth are consistent with the measured values on the glass substrates. The fabricated conductor-backed coplanar waveguides show insertion losses of 0.2 –0.3 dB/mm with a channel length of 1.86 mm, and the fabricated antennas have more than around 6% bandwidth in the frequency range of 35 to 39 GHz.**

Keywords-component; 5G component; co-planar waveguide; microstrip-fed single patch antenna; glass package

I. INTRODUCTION

Fifth-generation (5G) wireless communication standards have been emerging mainly because of three market drivers. One of them is the escalating consumer demand for gigabit wireless communications, for example, video and immersive multimedia [1-3]. The second is the Internet of things (IoT) technologies connecting everything from self-driving vehicles, robots, and jet-engine diagnostics, which produce vast information and therefore entail wide bandwidth [4]. The other driver is virtual reality that enables people feel the presence of each other [5].

To realize these trends, major advances in devices, packaging technologies, and device-package co-integration in the mm-wave frequency range are required [3, 6-7]. These technologies need to address key technical challenges such as increased loss, dominating role of interconnection parasitics and reduced radiation efficiency of antenna arrays [6, 8].

Both academia and industry have been exploring a wide variety of integration technologies to realize 5G communications [8]. State-of-the-art mm wave packages employ ceramics, organic laminates, and fan-out packages with mold compounds [9]. Ceramics are preferred for 5G applications because of their low loss, low moisture absorption, and stable properties in mm wave range and availability. The cost and integration limitations of ceramics led to the evolution of organic packages. A fully-integrated antenna-in-package (AiP) solution for W-band scalable phased-array systems is demonstrated by IBM [10 – 11]. A fully operational compact W-band transceiver package with 64 dual-polarization antennas was embedded in a multilayer organic substrate. Ultra-low loss organics based on Teflon and liquid-crystal polymers (LCP) were explored by VTT-Finland, with gains as high as 23 dBi and operational bandwidth of 2 GHz [11].

The evolution of embedded wafer fan-out packaging (EWFO), also referred to as embedded wafer-level ball grid array (eWLB) or fan-out wafer-level packaging (FO-WLP), further enhanced the performance or organic mm-wave packages. EWFO eliminates the use of wire bonding, which not only introduces significant radio frequency loss, but also increases the footprint for high-pin count die. Significantly reduced parasitics is the main advantage of eWLB compared to the standard BGA-wirebond and BGA flip-chip packages [12]. The transceiver bare die is embedded in a reconfigured molded wafer with compression molding process. Double-sided multiple redistribution layers are formed to fan-out the transceiver input/output signals, and through-mold vias are employed to realize the vertical interconnections. A fan-out eWLB with SiGe-BiCMOS technology was demonstrated by Infineon technologies [13]. Chang *et. al*., from IME Singapore, demonstrated a 3-D integrated 77-GHz automotive radar front-end [14].

For optimal performance, the patch antenna topologies typically need to be integrated on the substrate with active circuits using low-loss interconnects and feedlines [8, 10 – 11, 14 – 17]. State-of-the-art mm-wave modules cannot handle precision and tolerance for mm-wave components

approaching the dimensions of a few microns [8]. Glass-based packages are emerging as ideal candidates to realize mm-wave technologies because of their superior dimensional stability, availability in large-area low-cost panels, ability to form fine-pitch through-vias, stability to temperature and humidity, and matched coefficient of thermal expansion (CTE) with devices [18] along with low dielectric loss compared to silicon and mold compounds used in fan-out packages. To demonstrate the advantages of glass packages in 5G frequency bands, the fundamental electrical performance characteristics of 100 µm glass packages are investigated by modeling, design, simulation, and characterization of transmission-line structures and on-package antennas.

The first part of this paper analyzes transmission-line structures on 100 µm glass substrates with low-loss dielectric build-up materials for their insertion loss. Moreover, to show the capability of miniaturized antennas, the second part of this paper describes highly-efficient antenna topologies on glass substrates for multiple frequency bands and the impact of process variation on their performance.

II. Modeling and Design of MM-Wave Transmission Lines and Antenna Structures

The objective of this task is to demonstrate mm-wave components on glass with low-loss build-up materials, and analyze the model-to-hardware correlations. Simulations of transmission lines and antennas were performed from 28 GHz through 40 GHz. Such transmission lines have been widely used to demonstrate the low-loss properties of glass and other traditional substrates. This paper especially focuses on co-planar waveguides (CPWs) as transmission lines on thin glass substrates, which provide lower radiation loss than microstrip structures. For antenna structures, single patch antennas led by feedlines and a signal port are employed for a wide variety of frequency bands on 100 µm thick glass substrates.

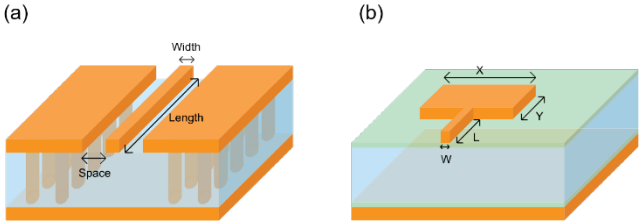

Figure 1. Configurations of (a) CB-CPW and (b) single-patch antenna

A. *Conductor-Backed Coplanar Waveguides*

In order to enable the high performance of antennas and distributed passives in a 5G package, low-loss interconnections and feedlines play a significant role. This section begins with the design of conductor-backed co-planar waveguides (CB-CPWs) with through-package vias (TPVs) of 30 µm diameter in a 100 µm glass substrate. CPWs, in general, provide lower conductor loss, dispersion, and smaller radiation loss at discontinuities, minimizing crosstalk on the same metallization layer [9, 19]. Moreover, CB-CPWs give lower-impedance transmission lines and higher structural strength [20]. To characterize the insertion loss per unit length, three types of CB-CPWs with various lengths were modeled and designed. In the designs, a 100 µm glass as a core substrate and TGVs with a diameter of 60 µm were assumed. The configuration, as shown in Fig. 1 (a), is determined and optimized with a 3D full-wave EM simulator considering fringing effects, and each dimension is tabulated in Table I. These CB-CPW structures have a ground line along with the signal line as shown in Fig. 1 (a), and the ground lines are connected to TGV arrays with 60 µm diameter so that better ground termination is realized. By placing TGV arrays, less coupling between transmission lines is achieved, leading to higher isolation from the electromagnetic interference generated by adjacent noise sources such as transmission lines or interconnections.

TABLE I. Dimensions of Three Types of CB-CPWs

Parameters	Width	Space	Length
Quarter long CB-CPW	181 µm	7 µm	0.42 mm
Half long CB-CPW			0.90 mm
Full long CB-CPW			1.86 mm

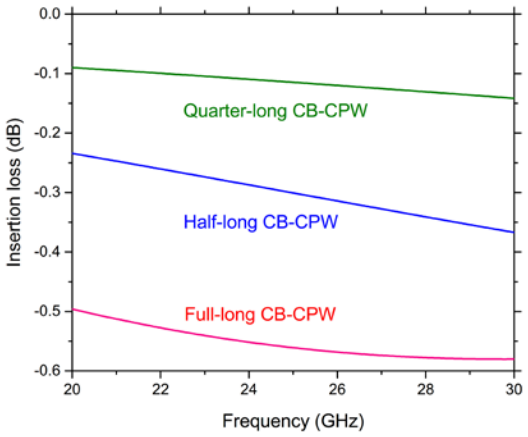

Figure 2. Simulated insertion loss of three different lengths of CB-CPWs as a function of frequency

The EM-simulated frequency responses (i.e., S-parameters), which are generated with HFSS and illustrated in Fig. 2, show that CB-CPWs over a 100 µm glass substrate provides 0.31 – 0.38 dB/mm. This result is attributed to the dielectric constant (5.0 – 5.4), and loss tangent (0.007), of the glass core. However, the simulations do not take the metal and dielectric surface roughness into account. The roughness or adhesion at dielectric-conductor interfaces create significant conductor losses that simulations do not detect. From the perspective of transmission lines with high precision, tolerance, and low loss, a 100 µm glass core, which enables smooth copper surface, is chosen in this paper.

B. *Single-Patch Antennas*

Wide-band phase-shifting networks with patch antenna array is another key class of mm wave components. In general, grouping antenna elements together results in several advantageous properties such as higher directivity compared to a single antenna element. For the best system performance, the antenna needs to be integrated onto the substrate with active circuits using low-loss interconnections and feedlines. Glass enables transmission lines with high precision, tolerance and low loss for miniaturized antenna array module with double-side thinfilm components. Four single-patch antennas with different center frequencies are employed in this paper, which begins with the design of single patch antennas for a variety of center frequencies from 37.5 GHz to 39.0 GHz with 3-dB bandwidths of 6.4 – 6.7%. The dimensions of the designed single-patch antennas are tabulated in Table II, and their simulated frequency responses are depicted in the Fig. 3.

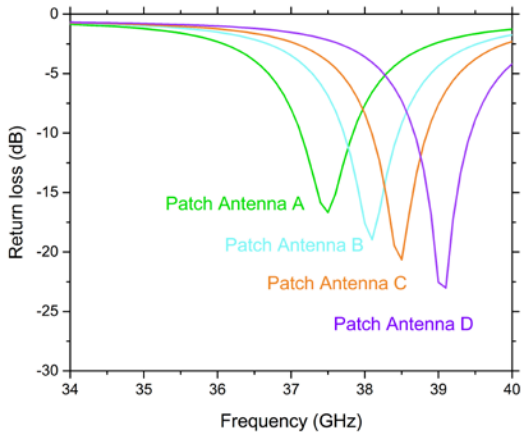

Figure 3. Reflection loss of four different types of single-patch antennas as a function of frequency

TABLE II. DIMENSIONS OF FOUR TYPES OF SINGLE PATCH ANTENNAS

Antenna	Center Frequency	Patch		Feedline	
		X (µm)	Y (µm)	W (µm)	L (µm)
Patch A	37.5 GHz	2170	1800	29	1033
Patch B	38.0 GHz		1770		
Patch C	38.5 GHz		1750		
Patch D	39.0 GHz		1720		

III. FABRICATION OF THE MM-WAVE STRUCTURES

Glass (SGW3 amd Grade EN-A1) with prefabricated vias are obtained from Corning Inc. and Asahi Glass Co., respectively. Appropriate handling procedures are required for glass substrate fabrication process in order to address the brittleness and fragility of ultrathin glass [21]. Polymer lamination on glass is the key to address the challenges with glass handling and metallization of smooth glass surfaces. Low-modulus polymer also acts as a buffer layer that reduces the stress from high CTE copper on glass. Polymer films also enable metallization by acting as an adhesion-promoting layer between electroless copper and glass. In addition, polymer acts as a barrier to prevent copper migration on glass surface between high density wiring under electrical bias.

The glass panels are treated with silane to increase adhesion, and prevent delamination during subsequent wet processes. Ajinomoto's GY-11 organic dry films with low dielectric loss of 0.0042 (5.8 GHz) are used in this test vehicle. Polymer lamination was performed with a vacuum laminator, followed by polymer curing. On the laminated polymer, a copper seed layer with a thickness of 0.2 µm is uniformly deposited through electroless plating. Adhesion of electroless copper to polymer is improved by prior roughening of the polymer surface using a permanganate chemical etch to create mechanical anchor sites. The wet chemical etch also cleans the residual polymer that is left on the nearby copper during via drilling processes. Metallization of top and bottom most metal traces and microvias is performed using a semi-additive patterning (SAP) process. Unlike a subtractive patterning, where a thick copper foil is etched off from the undesired areas to form circuit patterns, SAP yields better dimensional and copper sidewall control. This is because SAP avoids the long etching and lateral undercut that is usually prevalent during subtractive etching.

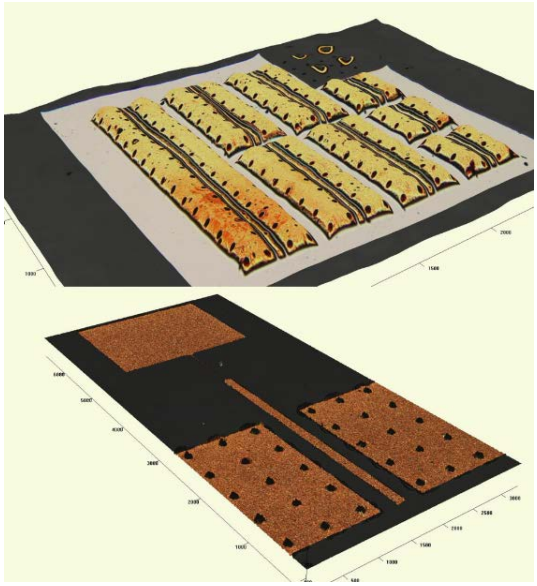

Figure 4. Fabricated 5G elements: (a) three types of CB-CPWs (b) a single-patch antenna

SAP starts with a photolithography step to create micromold patterns of CB-CPWs and single-patch antennas. A 15-µm dry film UV photoresist that can be patterned with an aqueous developer is employed. Photoresist adhesion strength and the planarity of the substrate can affect the lithography [21]. After the photolithography patterning process, the samples are subjected to 10-minute plasma etching in a chamber filled with O_2 gas to remove photoresist

remnants and improve the wettability of copper. Since the thickness of copper is targeted to be 8 µm, the authors strive to obtain 8.2 µm thickness totally, considering the removal of the seed layer at the end of this fabrication process. The photoresist is removed with a stripping solvent, after which the copper seed layer is etched as the last step to obtain the designed mm wave structures. The fabricated structures have a thickness of 8 ± 1 µm over the glass substrates. The fabricated structures of a CB-CPW and a single-patch antenna are depicted in Fig. 4.

IV. Characterization and Analyses

This section describes the characterization results from CB-CPWs and single-patch antennas that are fabricated on glass substrates. Electrical performance is evaluated from the scattering parameters measured after SOLT calibration through a vector network analyzer (VNA) in the frequency range of 20 GHz to 40 GHz.

A. Conductor-Backed Coplanar Waveguides

The electrical performance of the CB-CPWs is characterized by the insertion loss (IL), which represents the magnitude of the transmission coefficient S21 in the decibel scale. Three coupons from the quarter-long CB-CPW structure, three coupons from the half-long structure, and two coupons from the full-long CB-CPW are employed for the measurements. Fig. 5 shows the measurement results of the insertion loss of three types of transmission lines (i.e., quarter-long, half-long, full-long CB-CPWs). Table III shows the insertion losses at 28 GHz from measurements and compares them with the simulated values.

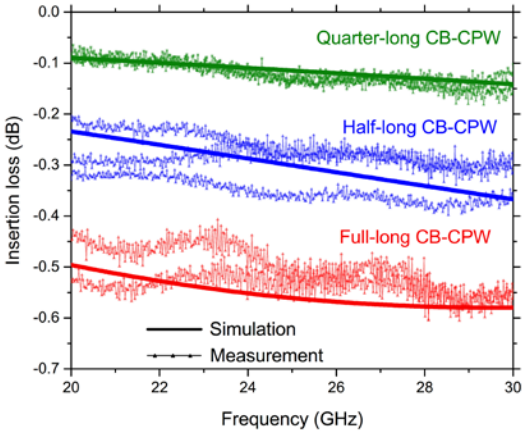

Figure 5. Measurement results of insertion loss of the fabricated CB-CPWs

TABLE III. Measured Results of Insertion Loss of the Fabricated CB-CPWs at 28 GHz

Parameters	Simulations		Measurements	
	IL (dB)	IL (dB/mm)	IL (dB)	IL (dB/mm)
Quarter long	-0.131	-0.311	-0.126	-0.274
			-0.138	-0.301
			-0.154	-0.334
Half long	-0.341	-0.355	-0.300	-0.337
			-0.364	-0.422
			-0.307	-0.322
Full long	-0.578	-0.311	-0.544	-0.293
			-0.567	-0.305

As shown in Table III, the measurement results from the eight coupons show agreement with the simulated frequency responses shown in Figs. 2 and 5. Minor discrepancies observed in the half-long and full-long CB-CPWs result from the deviations in the fabricated geometries from the designs. For transmission lines that are shorter in terms of their electrical length, process-related deviations in the geometry of transmission lines do not cause implausible discrepancy. However, for long transmission lines, the deviation in the geometries of the fabricated transmission lines from designed ones (Table IV) lead to unacceptable discrepancy, especially in the 20 – 30 GHz frequency range. One of the key reasons is the electrical wavelength; since the electrical wavelength at 28 GHz in a conductor such as copper is 10.7 mm, the electrical length of the full-long CB-CPWs is almost equivalent to the quarter wavelength. Therefore, in this frequency range, the change in geometries cause disagreement of RLGC parameters used in 3D full-wave simulations, leading to more discrepancy in longer CB-CPWs.

TABLE IV. Geometry Comparison between Designs and Fabrication for CB-CPWs

Parameters	Width (µm)		Space (µm)		Length (mm)	
	Design	Actual	Design	Actual	Design	Actual
Quarter	44	37.2	7	13.3	0.420	0.417
Half		38.0		12.7	0.900	0.898
Full		37.5		13.4	1.860	1.858

B. Single-Patch Antennas

The electrical performance of the CB-CPWs is characterized by the return loss (RL) measurements, which represents how well the input impedance of the network is matched with the nominal system impedance. This value is evaluated by S_{11} in decibels. The measured frequency responses of the four single patch-antennas are depicted in Fig. 6, along with the simulation results. Three coupons from each single-patch antenna (A,B, C, and D) are measured and illustrated in Fig. 6. The coupons cannot be differentiated from each other as they show similar frequency responses. In addition, 3-dB bandwidths of Patch Antenna A, B, C, and D are 6.40%, 6.28%, 5.52%, and 5.50%, respectively. However, center-frequency shifts are observed in Fig. 6, where the

magnitude of the shift is 1.40 GHz, 1.22 GHz, 1.41 GHz, and 1.38 GHz toward lower frequencies for Patch Antenna A, B, C, and D, respectively. Such frequency shifts in the center-frequencies are not acceptable for 5G designs.

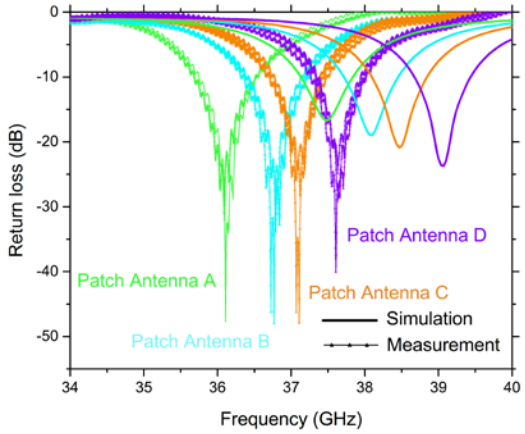

Figure 6. Measurement results of insertion loss of the fabricated single-patch antennas

To identify the origin of shifts shown in Fig. 6, each dimension is measured and tabulated against the designed dimensions in Table V. Moreover, the frequency responses with the measured geometries are re-simulated through 3D full-wave EM simulators and are shown in Fig. 7. The re-simulations produce favorable agreement with the measurement results.

From the re-simulations, it was found that the change in the geometries of feedlines is not as influential, while that of patch antennas strongly affect the center- or resonant frequency shift. In particular, the shrinkage of the patch length (Y) is the most influential factor of the four geometry factors. These results are compiled in Table V.

TABLE V. GEOMETRY COMPARISON BETWEEN DESIGNS AND FABRICATION FOR SINGLE PATCH ANTENNAS

Parameters	**Antenna A**		**Antenna B**	
(μm)	**Designed**	**Actual**	**Designed**	**Actual**
X	2170	2164	2170	2163
Y	1800	1791	1770	1763
W	29	23.7	29	24.5
L	1033	1039	1033	1045
Parameters	**Antenna C**		**Antenna D**	
(μm)	**Designed**	**Actual**	**Designed**	**Actual**
X	2170	2164	2170	2162
Y	1750	1742	1720	1711
W	29	23.7	29	23.9
L	1033	1044	1033	1041

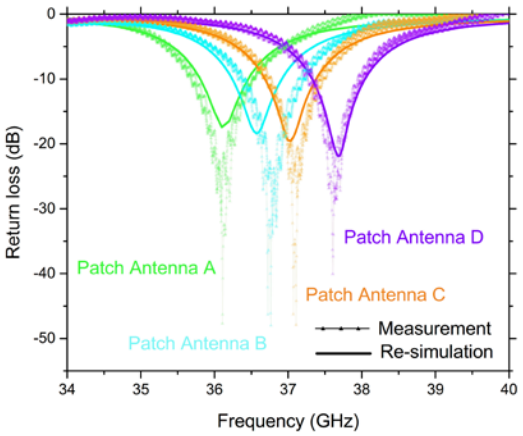

Figure 7. Re-simulated frequency responses after consideration of the geometry changes

V. CONCLUSION

A new class of substrate technologies with embedded actives, advanced antennas, and transmission lines with ultra-short interconnection lengths to actives are needed to realize 5G systems. Glass-based packages are emerging as ideal candidates to realize mm-wave technologies mainly because of their superior dimensional stability to realize fine-pitch multilayered RDL, low loss, availability in large-area low-cost panels, ability to form fine-pitch through-vias, stability to temperature and humidity, and matched CTE with devices. Glass-based transmission lines and patch antenna components were demonstrated for 5G applications. CB-CPW structures showed low insertion loss of less than 0.2-0.3 dB/mm. Microstrip-fed patch antenna on 100 μm glass substrates showed high gain of more than 5%. Process-induced deviations were analyzed by correlating measurements with simulations.

ACKNOWLEDGMENT

The authors wish to acknowledge the industry sponsors of the consortia program at GT-PRC for their technical guidance and support.

REFERENCES

[1] R. W. Heath, "Millimeter Wave: The Future of Commercial Wireless Systems," *2016 IEEE Compound Semiconductor Integrated Circuit Symposium (CSICS)*, Austin, TX, 2016, pp. 1-4.

[2] A. O. Watanabe *et al.*, "Highly-Effective Integrated EMI Shields with Graphene and Nanomagnetic Multilayered Composites," *2016 IEEE 66th Electronic Components and Technology Conference (ECTC)*, Las Vegas, NV, 2016, pp. 206-210.

[3] B. H. Ku *et al.*, "A 77–81-GHz 16-Element Phased-Array Receiver With 50° C Beam Scanning for Advanced Automotive Radars," in *IEEE Transactions on Microwave Theory and Techniques*, vol. 62, no. 11, pp. 2823-2832, Nov. 2014.

[4] J. G. D. Hester and M. M. Tentzeris, "Inkjet-Printed Flexible mm-Wave Van-Atta Reflectarrays: A Solution for Ultralong-Range Dense Multitag and Multisensing Chipless RFID Implementations for IoT

Smart Skins," in *IEEE Transactions on Microwave Theory and Techniques*, vol. 64, no. 12, pp. 4763-4773, Dec. 2016.

[5] J. Streque, A. Talbi, P. Pernod and V. Preobrazhensky, "New Magnetic Microactuator Design Based on PDMS Elastomer and MEMS Technologies for Tactile Display," in *IEEE Transactions on Haptics*, vol. 3, no. 2, pp. 88-97, April-June 2010.

[6] F. Dielacher, M. Tiebout, R. Lachner, H. Knapp, K. Aufinger and W. Sansen, "SiGe BiCMOS technology and circuits for active safety systems," *Proceedings of Technical Program - 2014 International Symposium on VLSI Technology, Systems and Application (VLSI-TSA)*, Hsinchu, 2014, pp. 1-4.

[7] C. Wagner *et al*., "A 77GHz automotive radar receiver in a wafer level package," *2012 IEEE Radio Frequency Integrated Circuits Symposium*, Montreal, QC, 2012, pp. 511-514.

[8] W. T. Khan *et al*., "A V-band end-fire Yagi-Uda antenna on an ultra-thin glass packaging technology," *2015 European Microwave Conference (EuMC)*, Paris, 2015, pp. 618-621.

[9] W. T. Khan, J. Tong, S. Sitaraman, V. Sundaram, R. Tummala and J. Papapolymerou, "Characterization of electrical properties of glass and transmission lines on thin glass up to 50 GHz," *2015 IEEE 65th Electronic Components and Technology Conference (ECTC)*, San Diego, CA, 2015, pp. 2138-2143.

[10] X. Gu *et al*., "Enhanced multilayer organic packages with embedded phased-array antennas for 60-GHz wireless communications," *2013 IEEE 63rd Electronic Components and Technology Conference*, Las Vegas, NV, 2013, pp. 1650-1655.

[11] X. Gu *et al*., "A compact 4-chip package with 64 embedded dual-polarization antennas for W-band phased-array transceivers," *2014 IEEE 64th Electronic Components and Technology Conference (ECTC)*, Orlando, FL, 2014, pp. 1272-1277.

[12] G. Haubner, W. Hartner, S. Pahlke, and M. Niessner, "77GHz automotive RADAR in eWLB package: From consumer to automotive packaging,"*Microelectronics Reliability*, vol. 64, pp. 699-704, 2016.

[13] J. Bock and R. Lachner, "SiGe BiCMOS and eWLB packaging technologies for automotive radar solutions," *2015 IEEE MTT-S International Conference on Microwaves for Intelligent Mobility (ICMIM)*, Heidelberg, 2015, pp. 1-4.

[14] K. F. Chang *et al*., "77-GHz Automotive Radar Sensor System With Antenna Integrated Package," in *IEEE Transactions on Components, Packaging and Manufacturing Technology*, vol. 4, no. 2, pp. 352-359, Feb. 2014.

[15] X. Gu, A. Valdes-Garcia, A. Natarajan, B. Sadhu, D. Liu and S. K. Reynolds, "W-band scalable phased arrays for imaging and communications," in *IEEE Communications Magazine*, vol. 53, no. 4, pp. 196-204, April 2015.

[16] Y. Li and K. M. Luk, "Low-Cost High-Gain and Broadband Substrate-Integrated-Waveguide-Fed Patch Antenna Array for 60-GHz Band," in *IEEE Transactions on Antennas and Propagation*, vol. 62, no. 11, pp. 5531-5538, Nov. 2014.

[17] J. Säily, A. Lamminen, and J. Francey, "Low cost high gain antenna arrays for 60 GHz millimetre wave identification (MMID)," 2011 [Online]. Available: http://www.taconic-add.com/pdf/technicalarticles-- high_gain_antenna_mmid.pdf.

[18] J. Tong, V. Sundaram, A. Shorey and R. Tummala, "Substrate-integrated waveguides in glass interposers with through-package-vias," *2015 IEEE 65th Electronic Components and Technology Conference (ECTC)*, San Diego, CA, 2015, pp. 2222-2227.

[19] M. El Gibari, M. Hadjloum and H. Li, "Conductor-backed coplanar waveguide to microstrip transition on BCB polymer thin film with bandwidth over 60 GHz," *2015 International Conference on Microwave and Photonics (ICMAP)*, Dhanbad, 2015, pp. 1-2.

[20] P. Mondal and S. K. Parui, "Study of defected grounded structures on both normal and conductor-backed coplanar waveguide," *2016 International Conference on Microelectronics, Computing and Communications (MicroCom)*, Durgapur, 2016, pp. 1-4.

[21] H. Lu *et al*., "Design, Modeling, Fabrication and Characterization of 2–5 μm Redistribution Layer Traces by Advanced Semiadditive Processes on Low-Cost Panel-Based Glass Interposers," in *IEEE Transactions on Components, Packaging and Manufacturing Technology*, vol. 6, no. 6, pp. 959-967, June 2016.